HHS Public Access

Author manuscript

ACS Biomater Sci Eng. Author manuscript; available in PMC 2022 June 24.

Published in final edited form as:

ACS Biomater Sci Eng. 2021 October 11; 7(10): 4838–4846. doi:10.1021/acsbiomaterials.1c00926.

Antifungal Effect of Piezoelectric Charges on PMMA Dentures

Carolina Montoya,
Department of Oral Health Sciences, Kornberg School of Dentistry, Temple University, Philadelphia, Pennsylvania 19140, United States

Julia Kurylec,
Department of Oral Health Sciences, Kornberg School of Dentistry, Temple University, Philadelphia, Pennsylvania 19140, United States

Divyashri Baraniya,
Department of Oral Health Sciences, Kornberg School of Dentistry, Temple University, Philadelphia, Pennsylvania 19140, United States

Aparna Tripathi,
Department of Oral Health Sciences, Kornberg School of Dentistry, Temple University, Philadelphia, Pennsylvania 19140, United States

Sumant Puri,
Department of Oral Health Sciences, Kornberg School of Dentistry, Temple University, Philadelphia, Pennsylvania 19140, United States

Santiago Orrego
Department of Oral Health Sciences, Kornberg School of Dentistry, Temple University, Philadelphia, Pennsylvania 19140, United States; Bioengineering Department, College of Engineering, Temple University, Philadelphia, Pennsylvania 19122, United States

Abstract

Candida-associated denture stomatitis is a recurring disease affecting up to 67% of denture wearers. Poly(methyl methacrylate) (PMMA) remains the main material employed in the fabrication of dentures due to its desirable physical, mechanical, and aesthetic properties. However, the improvement of its antimicrobial properties remains a challenge. To address this need, we developed PMMA composite filled with piezoelectric nanoparticles of barium titanate ($BaTiO_3$) for therapeutic effects. *Candida albicans* biofilms were cultivated on the surface of the composites under continuous cyclic mechanical loading to activate the piezoelectric charges and to resemble mastication patterns. The interactions between biofilms and biomaterials were

Corresponding Authors: Sumant Puri Phone: +1-215-707-5984; sumantpuri@temple.edu; **Santiago Orrego** Phone: +1-215-707-3817; sorrego@temple.edu.

Author Contributions

C.M. contributed to the design, data acquisition, analysis, and interpretation and drafted the manuscript; J.K. contributed to data acquisition; A.T. contributed to design. DB contributed to data acquisition for RT-qPCR, analysis, and interpretation; S.P. contributed to design, analysis, and interpretation; S.O. contributed to design, analysis, interpretation, supervision, and conceptualization. All authors critically revised the manuscript. All authors gave their final approval and agree to be accountable for all aspects of the work.

The authors declare no competing financial interest.

The Supporting Information is available free of charge at https://pubs.acs.org/doi/10.1021/acsbiomaterials.1c00926.

evaluated by measuring the biofilm biomass, metabolic activity, and the number of viable cells. To explore the antifungal mechanisms, changes in the expression of genes encoding adhesins and superoxide dismutase were assessed using reverse transcription-polymerase chain reaction. With the addition of piezoelectric nanoparticles, we observed a significant reduction in the biofilm formation and interference in the yeast-to-hyphae transition compared to the standard PMMA. Moreover, we observed that the cyclic deformation of biomaterial surfaces without antifungal agents produced increased biomass, metabolic activity, and a number of viable cells compared to the static/no-deformed surfaces. Cyclic deformation appears to be a novel mechanobiological signal that enables pathogenicity and virulence of *C. albicans* cells with increased expression of the yeast-to-hyphae transition genes. The outcome of this study opens new opportunities for the design of antifungal dentures for improved clinical service and reduced need for cleaning methods.

Graphical Abstract

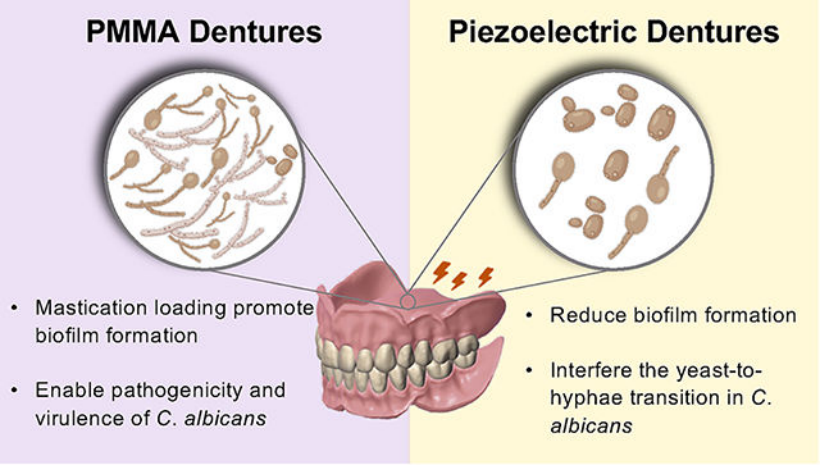

Keywords

antifungal; antimicrobial; PMMA; barium titanate; oral biofilms; oropharyngeal candidiasis; denture stomatitis; bioactive; C. albicans

1. INTRODUCTION

Candida albicans is an opportunistic fungus commonly found within the oral cavity. It adheres to oral surfaces like mucosa and acrylic dentures.[1] The excessive proliferation of *C. albicans* has been associated with denture-induced stomatitis (CADS).[2] CADS is a common recurring disease affecting up to 67% of denture wearers.[3] This disorder is characterized by the inflammation and erythema of the oral mucosal areas covered by the denture.[2] The incidence of CADS is higher among the elder, women, and immunosuppressed individuals.[4]

Etiological factors of CADS include bacterial and yeast contamination, accumulation of denture plaque (biofilms), the continual wearing of removable dentures, and poor denture hygiene.[2] CADS has a high rate of recurrence, even if treated with antifungal therapy.[5] Candida infection has been linked with periodontal diseases, oral/gastrointestinal/

pleuropulmonary infections, and even death.[6] Traditionally, antifungal agents are used to treating CADS, although other methods, including changes in denture-wearing patterns and denture cleaning/disinfection, are also used.[7] A major challenge is that *C. albicans* biofilms are highly resistant to antifungal drugs and host immune defenses due to complex biofilm architecture, accumulation of extracellular matrix, and increased expression of drug efflux pumps.[8,9] Additionally, the effectiveness of antifungal therapies is limited[2] since *Candida* biofilms are commonly embedded in denture imperfections that are hardly reachable by antifungal agents.[2] Antifungal treatment may eradicate *C. albicans* contamination; however, unless dentures are regularly maintained, cleaned, and decontaminated, CADS will recur when therapy is discontinued.[2]

Poly(methyl methacrylate) (PMMA) is a biomaterial commonly used in partial and complete dentures due to its physical and mechanical properties, ease of fabrication, and reduced cost.[10] A major limitation of PMMA is the lack of antifungal effects.[10] Biofilms easily colonize PMMA due to the absence of ionic charges, surface pores and irregularities, and the presence of electrostatic and hydrophobic interactions.[11] Surface pores and irregularities of the surface provide a larger surface area, facilitating bacteria colonization and biofilm maturation,[12,13] while microbes with hydrophobic cell surface have been found to favor biofilm formation in hydrophobic material surfaces like PMMA.[14]

Recently, the use of denture materials with antifungal properties has been proposed as one approach to control CADS and overcome the limitations of traditional antifungal therapies.[15,16] To prevent the formation of fungal biofilms over biomaterial surfaces, different strategies, including the release of antifungal ions and antibiotics and the use of anti-biofouling surfaces, have been proposed.[16–20] For example, denture materials incorporated with different antifungal agents, including cationic polymers (e.g., poly-(diallyldimethylammonium) chloride (PDDA)) and nanofillers (e.g., zinc oxide, silver, titanium dioxide, chitosan, copper, curcumin, graphene oxide).[21] Common limitations of these strategies include the short service life of antifungal agents due to leaching and the necessity of recharging.[22] In addition, the use of antimicrobials is limited since they cannot be administered for longer periods, as it often induces antimicrobial resistance and/or disrupts homeostasis of the microbiome.[23]

Piezoelectric materials produce electric charges in response to an applied mechanical load or vibrations (e.g., mastication loading). These smart materials have been successfully used in different biomedical applications, including drug delivery, tissue engineering, biosensors, and bone regeneration.[24–26] For example, our recent work showed that piezoelectric charges offer bioactivity by forming mineral layers in proportion to the magnitude of the electrical charge.[27] Piezoelectric materials have a significant advantage for therapeutical effects since electrical charges are produced continuously without the need for recharge for extended periods of time (e.g., +10 million cycles).[28] Barium titanate ($BaTiO_3$, BT hereafter) is a biocompatible piezoelectric ceramic commonly used for bone formation, cell proliferation, and differentiation.[29,30] This biomaterial has been tested in different forms, including nanoparticles and composites.[29,30] Our recent work revealed that piezoelectric charges from BT elicit antibacterial effects against Gram-positive bacteria.[31] We fabricated dental composites by adding barium titanate fillers (a biocompatible piezoelectric compound) into

standard dental resins (Bis-GMA/TEGDMA). The electrical charges prevented the bacterial biofilm formation and reduced the viable cells compared to control composites. However, we still do not know whether the same antibacterial mechanism can be applied to fungal species such as *C. albicans*. Little is known about the antifungal effects of piezoelectric charges. This research aims to investigate the antifungal effects of piezoelectric charges in the hope of understanding its antifungal mechanism and efficacy. Herein, we report that our piezoelectric PMMA composite exhibits antifungal activity in vitro. This new antifungal mechanism is expected to mitigate some of the limitations of current antifungal dental materials by harnessing mastication forces to activate the charges necessary to elicit the antifungal effects for extended periods of time.

2. MATERIALS AND METHODS

2.1. Fabrication of PMMA Piezoelectric Composites.

PMMA composites were fabricated first by mixing a commercial PMMA powder (Original Truliner, Bosworth) with 40 wt %. of barium titanate nanoparticles (US Research Nanomaterials US3830, 200 nm). The powders were mixed using a planetary mixer (ARE-310, Thinky) for 5 min at 2000 rpm. Then, the liquid monomer and the powders were mixed thoroughly by hand in a 1:1 weight ratio. The BT filler concentration was fixed at 40% (wt/wt) since it was the maximum packing fraction of BT within the matrix and provided a wide range of electrical charges for study. The mixture was then poured into a mold with the desired shape and was left for 10 min to complete autopolymerization. As a control group, samples without BT fillers were prepared. Samples were stored in distilled water for 24 h at 37 °C before testing to release uncured monomers. The average roughness of the surface was verified to be <0.2 μm to prevent influences on the biomaterial–biofilm interactions (see Appendix-1). Before testing, samples were subjected to a high electric field (20 kV/mm) at 140 °C for 40 min (poling) to improve the efficiency of charge generation without affecting the properties of the polymer[32] (Appendix-2).

2.2. Physical, Mechanical, and Electromechanical Characterization.

The PMMA composites and the control were characterized for their physical, mechanical, electromechanical, and wettability properties. The filler distribution was evaluated by scanning electron microscopy (SEM). In addition, the chemical composition and the degree of conversion (DC) were measured using Fourier transform infrared-attenuated total reflection (FTIR-ATR). The DC was determined from the ratio of the absorbance at the aliphatic C=C (1638 cm^{-1}) and the carbonyl C=O (1720 cm^{-1}) bonds for both polymerized and unpolymerized states. Second, the mechanical properties were determined using a three-point bending configuration following the ISO 20795–1 for denture materials. Flexural strength (σ) and modulus (E) were calculated. Third, the electromechanical properties (i.e., electrical charge generation in response to applied mechanical stress) were measured. Samples were subjected to cyclic loading under a 3-point bending resembling mastication patterns (stresses of ~22 MPa, frequency of 2 Hz). A charge amplifier was connected to conductive electrodes bonded in the sample located at the compressive and tension surfaces. The electrical charge and mechanical load were recorded (Appendix-2). Fourth, the contact

angles were evaluated (Appendix-3). For all evaluations, $N = 5$ samples per group were tested.

2.3. *C. albicans* Biofilm Model.

The *C. albicans* strain (CAI4) was grown on a yeast extract peptone dextrose (YPD) (DF0428, Thermo Fisher) agar plate at 30 °C for 24 h under aerobic conditions. A single colony was harvested and suspended in 10 mL of YPD media and grown at 30 °C with continuous shaking for 20 h. The fungal suspension was then diluted to $OD_{600} = 1.0$ in phosphate-buffered saline (PBS) (1×10^8 CFU/mL). Sterilized rectangular beams ($5 \times 1 \times 18$ mm^3) were submerged in 3 mL of the PBS/cell suspension oriented with the negatively charged surface upward (i.e., compression) and incubated at 37 °C for 3 h to promote cell adhesion to the sample surface. Then, the samples were gently washed with PBS to remove the nonadherent cells. Next, the beams were placed in a 3-point bending fixture (span: 15 mm) and submerged in 3 mL of RPMI 1640 (R1383, Sigma-Aldrich) supplemented with 1.5% agar (BP1423, Fisher Scientific) and 2% glucose (G8270, Sigma-Aldrich) and buffered with MOPS at pH 7.0 (M3183, Sigma-Aldrich). Then, the samples were incubated at 37 °C, and the cyclic loading was initiated for 24 h (Figure 2a). During the experiment, the load magnitude was adjusted to vary from −0.5 N to −5N(~22 MPa). This load magnitude enables a totally stable surface for the biofilm growth and does not create any surface defects on the samples (Appendix-4).[33] After the incubation period, the growth medium was removed, the side surfaces of the beam were gently cleaned, and the samples were washed with PBS.

2.4. Biofilm–Biomaterial Evaluations.

Cell viability was assessed by counting the number of colony-forming units (CFU). Six 10-fold serial dilutions were prepared and plated on YPD agar plates for 24 h at 30 °C under aerobic conditions. To assess the *C. albicans* biofilm biomass and metabolic activity, crystal violet and MTT assays were used, respectively, following previous protocols.[34] To visualize and quantify the living and the dead bacteria on top of the samples, the biofilm was stained using the LIVE/DEAD BacLight viability kit (Thermo Fisher L7007) (6 μM for SYTO 9 and 30 μM for propidium iodide). The live and dead cells were observed using a fluorescence microscope (EVOS M5000) (Appendix-5). Fluorescence images were collected as a set of 50 z-stack traversing the biofilms. All images and stacks were captured with identical settings. All intensities were corrected for background fluorescence. To quantify the proportion of live and dead yeast, the color images were converted to grayscale images with pixel values from 0 to 255. Then, a similar threshold was applied to obtain black and white images. All pixels with values above the threshold (white pixels) were counted. The number of white pixels was computed separately for both live and dead images. To estimate the biofilm biovolume, we manually revised all of the images within the z-stack. We identified the first (lower boundary) and last (upper boundary) images showing appropriate fluorescence. The level of biofilm was calculated by multiplying the number of images within the identified range over the z-stack thickness. Data analysis and measurement of the biofilm thickness were performed using ImageJ. For each evaluation, four samples ($N = 4$) per group were tested. The yeast-to-hyphae transition was monitored under a light microscope after 4 h of biofilm growth under cyclic mechanical stimulation. The hyphae

formation (%) was calculated as the ratio of the number of cells with germ tubes and the number of total cells at six random locations.

2.5. RNA Extraction and Gene Expression Assays.

RNA was extracted from biofilms after the 24 h incubation period using the RNeasy Mini Kit (QIAGEN) according to the manufacturer's instructions. RNA yield and quality were assessed using a NanoDrop (Thermo Fisher Scientific). Later, cDNA synthesis was performed using the iScript Reverse Transcription Supermix (Bio-Rad), following the manufacturer's protocol, and the contaminating DNA was digested using TURBO DNA-free kit (Invitrogen). Real-time PCR was performed using a QuantStudio TM 3.0 Real-time PCR system (Applied Biosystems) and the iTaq Universal SYBR Green supermix (Bio-Rad) with predesigned primer genes associated with *C. albicans* biofilm, including *ALS1, HWP1, GSC1*, and *SOD5*.[35,36] *18s rRNA* was used as a housekeeping gene[37] (Appendix-6). The reverse transcription-polymerase chain reaction (RT-qPCR) was performed at 95 °C for 5 min, followed by 40 cycles of 15 s at 95 °C and 1 min at 58 or 55 °C, depending on the primers used. The standard curve method was employed for relative quantitation, and genomic DNA was used to prepare a standard plot. Genomic DNA was extracted using the YeaStar Genomic DNA Kit (Zymo Research) after *C. albicans* was routinely grown in the YPD medium overnight.

2.6. Statistical Analysis.

All data are expressed as the mean ± standard deviations. Statistical differences in the results were evaluated using one-way ANOVA with a significance of 0.05. The Tukey post hoc test was used for multiple comparisons with a 95% confidence level.

3. RESULTS

A micrograph of the fracture surface of a selected piezoelectric composite sample is presented in Figure 1a. Piezoelectric fillers are distributed along the PMMA matrix without preferential deposition and with scattered agglomerations of sizes up to 9 μm. FTIR analysis confirmed the presence of BT and PMMA by showing their characteristic peaks at 530 and 1437 cm^{-1}, respectively (Figure 1b). The DC was found to be similar in both groups, with an average of ~73% (Figure 1c). The flexural strength and modulus are presented in Figure 1d,e, respectively. The average flexural strength of the piezoelectric composites (~50 MPa) was statistically lower than that of the control (~65 MPa). Conversely, the flexural modulus of both groups was statistically similar, with an average of 1.8 GPa. This decrease in the mechanical properties has been previously reported for PMMA composites filled with high concentrations of nanoparticles and could be influenced by the filler distribution, particle size, and shape.[38] The electrical charge density produced at the surface of the composites is shown in Figure 1f. As expected, no electrical charge was recorded for the PMMA group. On the contrary, higher charge density (~8.5 pC/cm^2) was measured for the piezoelectric composites simulating mastication stress conditions (22 MPa, 2 Hz).

The interactions between *C. albicans* biofilms and biomaterials were evaluated under two loading conditions, including samples under continuous cyclic loading and no loading

(held static without mechanical stimulation). Activation of the cyclic mechanical loading promoted in the PMMA samples a significant increase of biofilm biomass (Figure 2b), metabolic activity (Figure 2c), and viable cells (Figure 2d) compared to the PMMA no-load group. Under the same cyclic loading, piezoelectric composites showed a significant decrease in all microbiological evaluations (biomass, metabolic, and viable cells) compared to the commercial PMMA-loaded group, suggesting the activation of antifungal effects caused by the electric charges. Overall, the lowest biofilm biomass, metabolic activity, and CFU were observed for the PMMA no-load configuration. These findings were validated using fluorescence microscopy (Figure 2e). The highest number of live cells (green) was observed for the PMMA-loaded group (98%). An increased number of dead (red) fungal cells were observed in piezoelectric composites under mechanical loading (55%) compared to PMMA (1.7%). A similar trend was observed for the biofilm biovolume. Thicker biofilms were observed for the PMMA-loaded group, with a biovolume of 181 $\mu m^3/\mu m^2$. A reduction of 43% in the biofilm biovolume was observed for the mechanically stimulated piezoelectric composites (102 $\mu m^3/\mu m^2$).

Microscopic examination of the yeast-to-hyphae transition showed fully developed and robust hyphae in PMMA-loaded samples only (Figure 3b). In contrast, in the other groups, spherical yeast cells (Figure 3c) or/and oval and elongated pseudohyphae cells predominated (Figure 3a,d). This suggests that the addition of BT to the PMMA and the resulting mastication-induced electrical charges interfered with the morphological transition of *C. albicans* by inhibiting the formation of hyphae. These observations were further confirmed by the quantification of hyphae formation (Figure 3e). In the PMMA-loaded group, the incidence of yeast-to-hyphae transition was significantly higher (~88%) compared to the other evaluated groups (<20%).

To understand the mechanisms driving the changes of the biofilm–biomaterial interactions, the expression of *ALS1* for cell-surface associated glycoproteins, *HWP1* for hyphal-specific adhesion, *GSC1* for production of extracellular matrix (β-1,3-glucan synthase), and *SOD5* for superoxide dismutase production were investigated (Figure 4). Significant differences between all groups (PMMA and the piezoelectric composite for both loading conditions) were found in the expression of *ALS1* (Figure 4a) and *GSC1* (Figure 4c) genes with the highest levels for the piezoelectric-loaded cases. On the other hand, the expression of the *HWP1* gene was similar between the piezoelectric composite- and PMMA-loaded groups (Figure 4b). Interestingly, the expression of the *GSC1* and *SOD5* genes was highest for both piezoelectric composites and lowest for PMMA under loading conditions (Figure 4c,d).

4. DISCUSSION

Dentures with different antifungal agents have been proposed with the major limitation of offering short therapeutic action due to the leaching of agents.[15] In this work, we proposed the use of a novel antifungal mechanism by utilizing piezoelectric materials. Our material does not rely on antifungal drugs or leaching agents since piezoelectric materials can produce electrical charges from vibrations/cyclic loading for extended periods of time without the need for recharging.[28,39] For the first time, our work showed the antimicrobial effects of piezoelectric charges against *C. albicans* biofilms. In addition, for the first time,

our results showed that cyclic mechanical loading (i.e., a mechanobiology signal) is an environmental factor affecting the biofilm growth and morphology of *C. albicans* biofilms, evidenced with increased virulence, biomass, metabolic activity, and viable cells.

Microbe–surface interactions are affected by different biomaterial properties, including chemistry, roughness/topography, surface energy, and charge.[40] Specifically, for *C. albicans*, high hydrophobicity and surface roughness enhance the adhesion and proliferation of yeast.[41] In our work, we subjected PMMA samples to cyclic loading/deformation throughout the incubation period. This cyclic deformation of the biomaterial surface appears to have enabled the pathogenicity and virulence of *C. albicans*, as evidenced in different results. First, the increased levels of biomass, metabolic activity, and viable cells (Figure 2b–d), after comparing loaded and no-loaded groups. Second, cyclic loading contributed to the increased formation of hyphae (Figure 3e). This morphological switch between unicellular yeast and multicellular filamentous hyphal growth is known to play a role in the virulence of *C. albicans* evidenced with biofilm formation, phenotypic switching, and secretion of hydrolytic enzymes.[42,43] This yeast-to-hyphae transition is known to be regulated by a range of environmental and nutritional cues, including pH, CO_2, temperature, nutritional deprivation, and hypoxia.[42,43] However, it was not known that cyclic loading (mechanobiology signal) on biomaterial surfaces contributed to this morphological switch. This condition is critical, especially when evaluating fungi–biomaterial interactions in microenvironments, where repetitive loading is present, such as oral dentures and catheters.

To confirm this observation, we explored the regulation of specific genes. The upregulation of the *HWP1* gene is associated with the cell-wall protein that is required for normal hyphal development,[44] which was evidenced for all of the loaded groups (Figure 4b). In addition, the downregulation of the GSC1 gene suggests a decrease of the β-glucan levels after the yeast-to-hyphae transition (Figure 4c).[45] Moreover, the upregulation of the *ALS1* gene has been associated with the formation of biofilms (Figure 4a) with higher biomass and resistance to removal[46] (see Figure 2b). Taken together, the cyclic deformation of the PMMA surface contributed to an increased biofilm formation with increased hyphal production. Thus, the cyclic surface deformation is proposed as a new mechanosensing cue that triggers the transition from normal flora to pathogenic and opportunistic yeast infection. In simple terms, the act of eating using a denture appears to promote the yeast-to-hyphae transition, which enables the pathogenicity and virulence of *C. albicans*.

Electrostatic interactions influence the adherence of *C. albicans* to polymer surfaces.[47] The yeast cell wall is negatively charged by the phosphate and carboxyl groups.[48] Electrical charges at the biomaterial surface may alter the interaction with Candida cells.[47] Specifically, the prevention of cell adhesion is through the negative–negative charge interactions.[49] Piezoelectric fillers produce electrical charges (“repulsion forces”) on the biomaterial surface activated by cyclic loading. These repulsive interactions were evidenced by the lower levels of biofilm biomass, metabolism, and viable cells on the piezoelectric composite compared to PMMA-loaded samples (Figure 2). This type of electrostatic interaction causes the cell envelope to be displaced, leading to a loss of structural integrity and cell lysis, which also correlates with a higher number of dead cells.[50] Our fluorescence microscopy results confirm this by showing an increased number of dead cells in the

piezoelectric composites (see Figure 2e). Furthermore, the upregulation of the *ALS1* gene for the piezoelectric composite (Figure 4a) suggests that the antifungal mechanism is not related to reduced cell adhesion to the biomaterial surface. Taken together, the electrical charges produced by piezoelectric fillers are delaying the biofilm formation by inducing the death of cells without affecting the adhesion of cells on the surface of the biomaterial.

To explore the antifungal mechanism, we measured the expression of a superoxide dismutase gene (*SOD5*), which indicates both oxidative stress production and the yeast-to-hyphae transition.[51] The antimicrobial mechanism of compounds that generate electrical charges is through the induction of reactive oxygen species (ROS) production.[52,53] The elevation of intracellular ROS induces oxidative damage to proteins, lipids, and DNA, which leads to cell death.[54] Piezoelectric charges induced the upregulation of *SOD5* with minimal hyphae formation, suggesting that the antifungal mechanism could be related to oxidative stresses. However, the PMMA-loaded samples reported the high formation of hyphae with the downregulation of *SOD5*, indicating that the mechanical stimuli have an unknown effect on the superoxide dismutase gene function, which warrants further investigation. The increase of *SOD5* in the piezocomposite without cyclic loading appears to be related to the residual charge on the sample's surface. However, direct measurement of the ROS production is required. Additional studies regarding the molecular antifungal mechanism, gene expression patterns, and identification of pathways specific to pathogenic *C. albicans* biofilms are encouraged to elucidate the complete antifungal mechanism.

For the first time, our work showed the antimicrobial effects of piezoelectric charges against *C. albicans* biofilms. A reduction in the number of viable bacteria was observed after PMMA samples produced ~8 pC of electrical charge on the biomaterial surfaces. Despite the exciting results, this study has limitations. The experiments were performed in the absence of saliva pellicle, which can influence the adhesion dynamics of *C. albicans*. We utilized RPMI media, which could induce hyphal development.[55] Moreover, only one concentration of piezoelectric fillers was tested. Different nanoparticle concentrations, sizes, and surface treatments (i.e., silanization to improve mechanical properties) and distributions can render different mechanical properties, electrical charge magnitudes (Appendix-7), and thus, different microbiological and molecular responses (Appendix-8). Similarly, we choose one material (PMMA), one mechanical stress condition, and one strain of fungi. However, future studies should consider using a clinical inoculum that enables the study of the interactions between different microorganisms/pathogens after exposure to piezoelectric charges.[56] In addition, dental materials (Appendix-9) with different matrixes and cyclic loading parameters (stress/frequency) verifying the antifungal mechanism warrant further investigation. Additional studies regarding changes of patterns of gene expression and identification of pathways specific to pathogenic *C. albicans* biofilms are encouraged to elucidate the full antifungal mechanism of piezoelectric charges. Finally, a systematic study to evaluate higher magnitudes (>8 pC) of electrical charges on the antimicrobials should be considered. With that in mind, this study initiated the understanding of the complex interactions between *C. albicans*, piezoelectric charges, and cyclic mechanical deformation, which would provide a new perspective for developing new strategies for preventing and treating yeast infections.

5. CONCLUSIONS

For the first time, we propose the use of piezoelectric PMMA composites with antifungal effects for denture use. Our results showed that piezoelectric charges significantly reduced the biomass, metabolic activity, and viable cells compared to the commercial PMMA without charge generation. Piezoelectric charges also prevented the formation of hyphae. The antifungal mechanism from piezoelectric charges appears to be related to the accumulation of intracellular reactive oxygen species (ROS) and damage to the cell membrane. In addition, our results indicate that cyclic deformation on PMMA substrates without antifungal agents, where the biofilms were formed and yeast adhered, enabled pathogenicity and virulence of *C. albicans*. Cyclic loading alone contributed to an increased formation of biofilm with augmented hyphal production. We believe this is a new virulence mechanism that contributes to the progression of infection, which can be targeted for the development of new strategies for the treatment of yeast infections.

Supplementary Material

Refer to Web version on PubMed Central for supplementary material.

ACKNOWLEDGMENTS

The authors would like to thank Dr. Nezar Al-Hebshi, Dr. Anubhav Nahar, and Casey Rubin for their support throughout the project.

Funding

This work was supported in part by the National Institute of Dental and Craniofacial Research (NIDCR) Awards R21DE030564 (PI:Orrego) and R03DE026451 (PI:Puri). This work was also supported in part by the Temple University Maurice Kornberg School of Dentistry start-up fund and by the Office of Provost at Temple University strategic fund.

REFERENCES

(1). Cannon R; Chaffin W Oral Colonization by *Candida albicans*. Crit. Rev. Oral Biol. Med. 1999, 10, 359–383. [PubMed: 10759414]

(2). Gendreau L; Loewy ZG Epidemiology and Etiology of Denture Stomatitis. J. Prosthodontics 2011, 20, 251–260.

(3). Webb BC; Thomas CJ; Willcox MDP; Harty DWS; Knox KW Candida-Associated Denture Stomatitis. Aetiology and Management: A Review: Part1. Factors influencing Distribution of Candida Species in the Oral Cavity. Aust. Dent. J. 1998, 43, 45–50. [PubMed: 9583226]

(4). Prakash B; Shekar M; Maiti B; Karunasagar I; Padiyath S Prevalence of Candida spp. among Healthy Denture and Nondenture Wearers with Respect to Hygiene and Age. J. Indian Prosthodont. Soc. 2015, 15, 29–32. [PubMed: 26929483]

(5). Pereira CA; Toledo BC; Santos CT; Pereira Costa AC; Back-Brito GN; Kaminagakura E; Jorge AO Opportunistic Microorganisms in Individuals with Lesions of Denture Stomatitis. Diagn. Microbiol. Infect. Dis. 2013, 76, 419–424. [PubMed: 23747028]

(6). Golecka M; Oldakowska-Jedynak U; Mierzwińska-Nastalska E; Adamczyk-Sosińska E Candida-Associated Denture Stomatitis in Patients after Immunosuppression Therapy. Transplant. Proc. 2006, 38, 155–156. [PubMed: 16504690]

(7). Garcia-Cuesta C; Sarrion-Pérez M-G; Bagán JV Current Treatment of Oral Candidiasis: A Literature Review. J. Clin. Exp. Dent. 2014, 6, e576–e582. [PubMed: 25674329]

(8). Chandra J; Kuhn DM; Mukherjee PK; Hoyer LL; McCormick T; Ghannoum MA Biofilm Formation by the Fungal Pathogen *Candida albicans*: Development, Architecture, and Drug Resistance. J. Bacteriol. 2001, 183, 5385–5394. [PubMed: 11514524]

(9). Sandai D; Tabana YM; Ouweini AE; Ayodeji IO Resistance of *Candida albicans* Biofilms to Drugs and the Host Immune System. Jundishapur J. Microbiol. 2016, 9, No. e37385.

(10). Meirowitz A; Rahmanov A; Shlomo E; Zelikman H; Dolev E; Sterer N Effect of Denture Base Fabrication Technique on *Candida albicans* Adhesion In Vitro. Materials 2021, 14, No. 221. [PubMed: 35009178]

(11). Sivakumar I; Arunachalam KS; Sajjan S; Ramaraju AV; Rao B; Kamaraj B Incorporation of Antimicrobial Macromolecules in Acrylic Denture Base Resins: A Research Composition and Update. J Prosthodontics 2014, 23, 284–290.

(12). Teughels W; Van Assche N; Sliepen I; Quirynen M Effect of Material Characteristics and/or Surface Topography on Biofilm Development. Clin. Oral Implants Res. 2006, 17, 68–81. [PubMed: 16968383]

(13). Bollenl CML; Lambrechts P; Quirynen M Comparison of Surface Roughness of Oral Hard Materials to the Threshold Surface Roughness for Bacterial Plaque Retention: A Review of the Literature. Dent. Mater. 1997, 13, 258–269. [PubMed: 11696906]

(14). Zheng S; Bawazir M; Dhall A; Kim H-E; He L; Heo J; Hwang G Implication of Surface Properties, Bacterial Motility, and Hydrodynamic Conditions on Bacterial Surface Sensing and Their Initial Adhesion. Front. Bioeng. Biotechnol. 2021, 9, No. 643722.

(15). Makvandi P; Gu JT; Zare EN; Ashtari B; Moeini A; Tay FR; Niu L.-n. Polymeric and Inorganic Nanoscopical Antimicrobial Fillers in Dentistry. Acta Biomaterialia 2020, 101, 69–101. [PubMed: 31542502]

(16). Wen J; Yeh C-K; Sun Y Functionalized Denture Resins as Drug Delivery Biomaterials to Control Fungal Biofilms. ACS Biomater. Sci. Eng. 2016, 2, 224–230. [PubMed: 33418635]

(17). Vera-González N; Shukla A Advances in Biomaterials for the Prevention and Disruption of Candida Biofilms. Front. Microbiol. 2020, 11, No. 538602.

(18). AlBin-Ameer MA; Alsrheed MY; Aldukhi IA; Matin A; Khan SQ; Abualsaud R; Gad MM Effect of Protective Coating on Surface Properties and *Candida albicans* Adhesion to Denture Base Materials. J. Prosthodontics 2020, 29, 80–86.

(19). Černáková L; Light C; Salehi B; Rogel-Castillo C; Victoriano M; Martorell M; Sharifi-Rad J; Martins N; Rodrigues CF Novel Therapies for Biofilm-Based *Candida* spp. Infections. Adv. Exp. Med. Biol. 2019, 1214, 93–123. [PubMed: 31321751]

(20). Waterhouse A; Leslie DC; Lightbown K; Antonoff D; Lightbown S; Dimitrakakis N; Hicks-Berthet JB; Leslie CN; Super M; Ingber DE; Ackerman MB Rapid Coating Process Generates Omniphobic Dentures in Minutes to Reduce *C. albicans* Biofouling. ACS Biomater. Sci. Eng. 2019, 5, 420–424. [PubMed: 33405807]

(21). Ahmad N; Jafri Z; Khan ZH Evaluation of Nanomaterials to Prevent Oral Candidiasis in PMMA Based Denture Wearing Patients. A systematic analysis. J. Oral Biol. Craniofac. Res. 2020, 10, 189–193. [PubMed: 32373449]

(22). Lin DM; Kalachandra S; Valiyaparambil J; Offenbacher S A Polymeric Device for Delivery of Anti-Microbial and Anti-Fungal Drugs in the Oral Environment: Effect of Temperature and Medium on the Rate of Drug Release. Dent. Mater. 2003, 19, 589–596. [PubMed: 12901982]

(23). Langdon A; Crook N; Dantas G The Effects of Antibiotics on the Microbiome Throughout Development and Alternative Approaches for Therapeutic Modulation. Genome Med. 2016, 8, No. 39.

(24). Montoya C; Du Y; Gianforcaro AL; Orrego S; Yang M; Lelkes PI On the road to Smart Biomaterials for Bone Research: Definitions, Concepts, Advances, and Outlook. Bone Res. 2021, 9, No. 12.

(25). Zaszczyńska A; Gradys A; Sajkiewicz P Progress in the Applications of Smart Piezoelectric Materials for Medical Devices. Polymers 2020, 12, No. 2754.

(26). Tandon B; Blaker JJ; Cartmell SH Piezoelectric Materials as Stimulatory Biomedical Materials and scaffolds for Bone Repair. Acta Biomaterialia 2018, 73, 1–20. [PubMed: 29673838]

(27). Orrego S; Chen Z; Krekora U; Hou D; Jeon SY; Pittman M; Montoya C; Chen Y; Kang SH Bioinspired Materials with Self-Adaptable Mechanical Properties. Adv. Mater. 2020, 73, No. e1906970.

(28). Lin B; Giurgiutiu V; Pollock P; Xu B; Doane J Durability and Survivability of Piezoelectric Wafer Active Sensors on Metallic Structure. AIAA J. 2010, 48, 635–643.

(29). Acosta M; Novak N; Rojas V; Patel S; Vaish R; Koruza J; Rossetti G; Rödel J BaTiO3-Based Piezoelectrics: Fundamentals, Current Status, and Perspectives. App. Phys. Rev. 2017, 4, No. 041305.

(30). Kapat K; Shubhra QTH; Zhou M; Leeuwenburgh S Piezoelectric Nano-Biomaterials for Biomedicine and Tissue Regeneration. Adv. Funct. Mater. 2020, 30, No. 1909045.

(31). Montoya C; Jain A; Londoño J; Correa S; Lelkes P; Melo M; Orrego S Multifunctional Dental Composite with Piezoelectric Nano-Fillers for Both Antibiofilm and Remineralization Therapies. ACS Appl. Mater. Interfaces 2021, 13, 43868–43879. [PubMed: 34494813]

(32). Waller D; Safari A Corona Poling of PZT Ceramics and Flexible Piezoelectric Composites. Ferroelectrics 1988, 87, 189–195.

(33). Krsmanovic M; Biswas D; Ali H; Kumar A; Ghosh R; Dickerson AK Hydrodynamics and Surface Properties Influence Biofilm Proliferation. Adv. Colloid Interface Sci. 2021, 288, No. 102336.

(34). Camilleri J; Arias Moliz T; Bettencourt A; Costa J; Martins F; Rabadijeva D; Rodriguez D; Visai L; Combes C; Farrugia C; Koidis P; Neves C Standardization of Antimicrobial Testing of Dental Devices. Dent. Mater. 2020, 36, e59–e73. [PubMed: 31928776]

(35). Bink A; Vandenbosch D; Coenye T; Nelis H; Cammue BPA; Thevissen K Superoxide Dismutases are Involved in *Candida albicans* Biofilm Persistence Against Miconazole. Antimicrob. Agents Chemother. 2011, 55, 4033–4037. [PubMed: 21746956]

(36). Alonso GC; Pavarina AC; Sousa TV; Klein MI A Quest to Find Good Primers for Gene Expression Analysis of *Candida albicans* From Clinical Samples. J. Microbiol. Methods 2018, 147, 1–13. [PubMed: 29454005]

(37). Bakri MM; Cannon RD; Holmes AR; Rich AM Detection of *Candida albicans* ADH1 and ADH2 mRNAs in Human Archival Oral Biopsy Samples. J. Oral Pathol. Med. 2014, 43, 704–710. [PubMed: 24931506]

(38). Ali Sabri B; Satgunam M; Abreeza NM; N Abed A A Review on Enhancements of PMMA Denture Base Material with Different Nano-Fillers. Cogent Eng. 2021, 8, No. 1875968.

(39). Mohammed AA; Haris SM; Nuawi MZ Role of Piezoelectric Elements in Finding the Mechanical Properties of Solid Industrial Materials. Appl. Sci. 2018, 8, No. 1737.

(40). Song F; Koo H; Ren D Effects of Material Properties on Bacterial Adhesion and Biofilm Formation. J. Dental Res. 2015, 94, 1027–1034.

(41). Pereira-Cenci T; Del Bel Cury AA; Crielaard W; Ten Cate JM Development of Candida-Associated Denture Stomatitis: New Insights. J. Appl. Oral Sci. 2008, 16, 86–94. [PubMed: 19089197]

(42). Villa S; Hamideh M; Weinstock A; Qasim MN; Hazbun TR; Sellam A; Hernday AD; Thangamani S Transcriptional Control of Hyphal Morphogenesis in *Candida albicans*. FEMS Yeast Res. 2020, 20, No. foaa005.

(43). Thompson DS; Carlisle PL; Kadosh D Coevolution of Morphology and Virulence in Candida Species. Eukaryotic Cell 2011, 10, 1173–1182. [PubMed: 21764907]

(44). Orsi CF; Borghi E; Colombari B; Neglia RG; Quaglino D; Ardizzoni A; Morace G; Blasi E Impact of *Candida albicans* hyphal wall protein 1 (HWP1) Genotype On Biofilm Production and Fungal Susceptibility to Microglial Cells. Microbial Pathog. 2014, 69–70, 20–27.

(45). Mio T; Adachi-Shimizu M; Tachibana Y; Tabuchi H; Inoue SB; Yabe T; Yamada-Okabe T; Arisawa M; Watanabe T; Yamada-Okabe H Cloning of the *Candida albicans* Homolog of Saccharomyces cerevisiae GSC1/FKS1 and its Involvement in beta-1,3-glucan Synthesis. J. Bacteriol. 1997, 179, 4096–4105. [PubMed: 9209021]

(46). Jackson S; Coulthwaite L; Loewy Z; Scallan A; Verran J Biofilm Development by Blastospores and Hyphae of *Candida albicans* on Abraded Denture Acrylic Resin Surfaces. J. Prosthet. Dent. 2014, 112, 988–993. [PubMed: 24726593]

(47). Park SE; Periathamby AR; Loza JC Effect of Surface-Charged Poly(Methyl Methacrylate) on the Adhesion of *Candida albicans1*. J. Prosthodontics 2003, 12, 249–254.

(48). Orlean P Architecture and Biosynthesis of the Saccharomyces cerevisiae Cell Wall. Genetics 2012, 192, 775–818. [PubMed: 23135325]

(49). Klotz SA; Drutz DJ; Zajic JE Factors Governing Adherence of Candida species to Plastic Surfaces. Infect. Immun. 1985, 50,97–101. [PubMed: 3899942]

(50). Kügler R; Bouloussa O; Rondelez F Evidence of a Charge-Density Threshold for Optimum Efficiency Of Biocidal Cationic Surfaces. Microbiology 2005, 151, 1341–1348. [PubMed: 15870444]

(51). Martchenko M; Alarco AM; Harcus D; Whiteway M Superoxide Dismutases in *Candida albicans*: Transcriptional Regulation and Functional Characterization of the Hyphal-Induced SOD5 gene. Mol. Biol. Cell 2004, 15, 456–467. [PubMed: 14617819]

(52). Sultana ST; Babauta JT; Beyenal H Electrochemical Biofilm Control: A Review. Biofouling 2015, 31, 745–758. [PubMed: 26592420]

(53). Wang Y; Xu Y; Dong S; Wang P; Chen W; Lu Z; Ye D; Pan B; Wu D; Vecitis CD; Gao G Ultrasonic Activation of Inert Poly(tetrafluoroethylene) enables Piezocatalytic Generation of Reactive Oxygen Species. Nat. Commun. 2021, 12, No. 3508.

(54). Orrenius S Reactive Oxygen Species in Mitochondria-Mediated Cell Death. Drug Metab. Rev. 2007, 39, 443–455. [PubMed: 17786631]

(55). Ramage G; VandeWalle K; López-Ribot JL; Wickes BL The filamentation Pathway Controlled by the Efg1 Regulator Protein is Required for Normal Biofilm Formation and Development in *Candida albicans*. FEMS Microbiol. Lett. 2002, 214, 95–100. [PubMed: 12204378]

(56). Sztajer H; Szafranski SP; Tomasch J; Reck M; Nimtz M; Rohde M; Wagner-Döbler I Cross-feeding and Interkingdom Communication in Dual-Species Biofilms of Streptococcus mutans and *Candida albicans*. ISME J. 2014, 8, 2256–2271. [PubMed: 24824668]

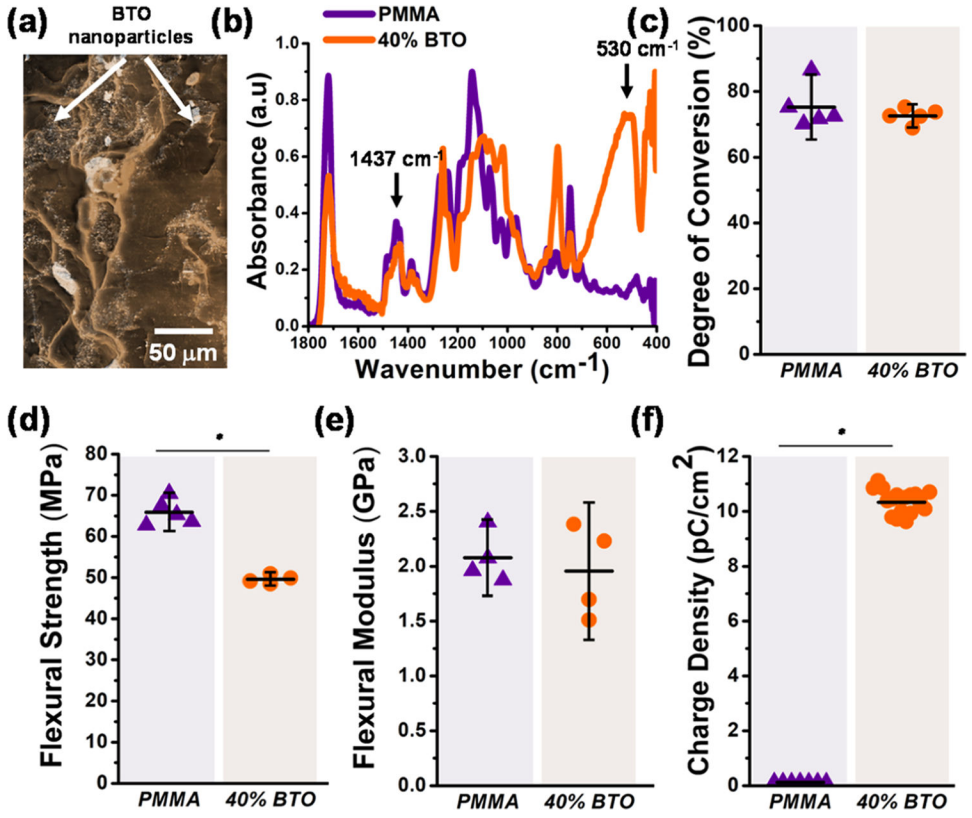

Figure 1.

Characterization of PMMA piezoelectric composites. (a) Micrograph of the fracture surface of a PMMA sample filled with 40% of BT. White arrows indicate piezoelectric fillers. (b) Selected FTIR spectra of the fracture surface of the commercial PMMA and the piezoelectric composite, indicating the characteristics peaks corresponding to the PMMA matrix (1437 cm^{-1}) and BT filler (530 cm^{-1}). (c) Degree of conversion of the commercial PMMA and the piezoelectric composites measured by Fourier transform infrared (FTIR) spectroscopy ($p = 0.4204$). (d) Flexural strength ($p = 0.000$) and (e) flexural modulus of the piezoelectric composites and the commercial PMMA ($p = 0.8055$). (f) Electrical charge density (Q per cm^2) generated by PMMA piezoelectric composites subjected to a three-point bending cyclic loading of 5 N at 2 Hz ($p = 0.000$). For all tests, the error bars were obtained from $N = 5$ samples. Significant differences between the groups are expressed as $*p < 0.05$.

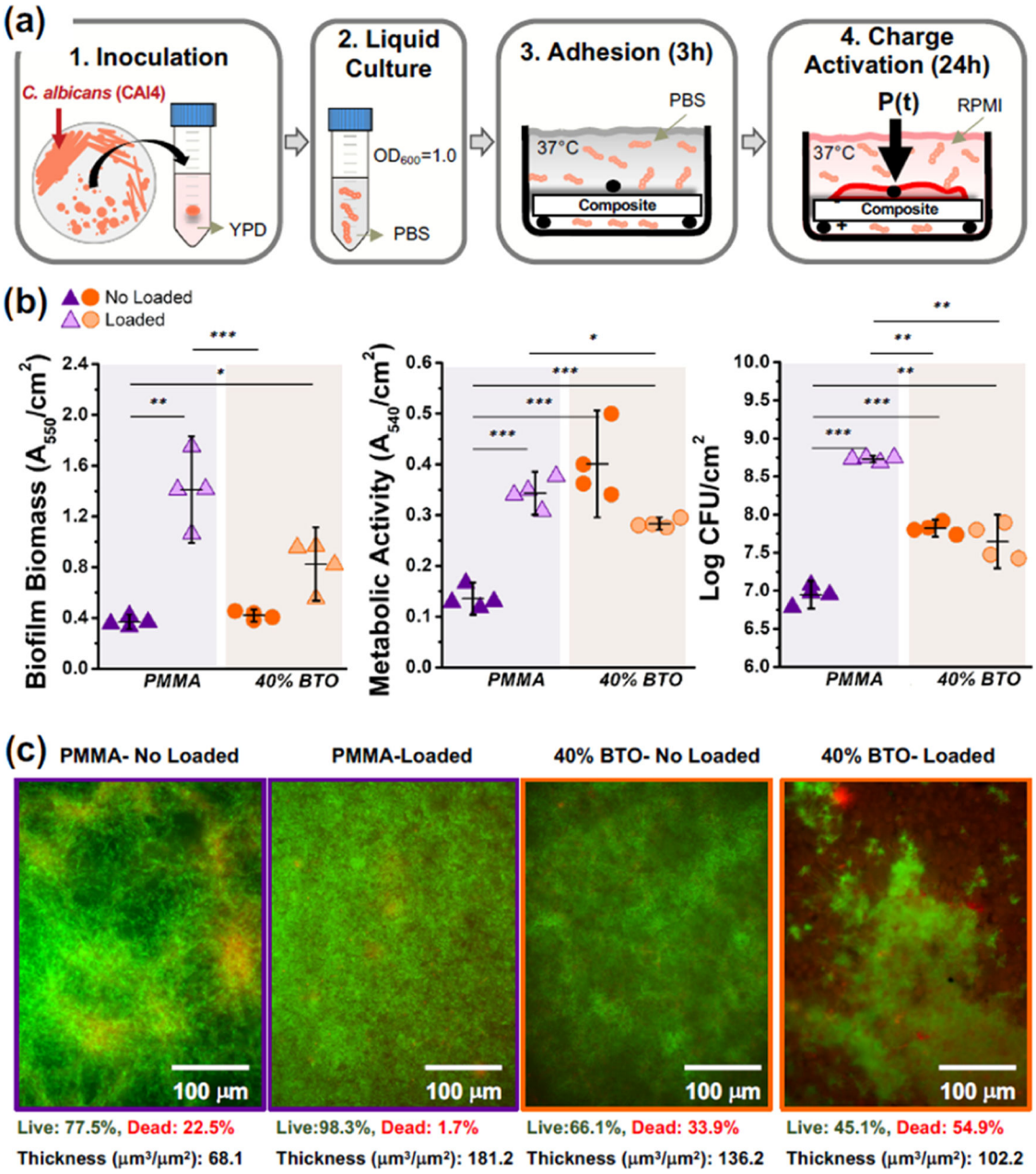

Figure 2.

Biofilms–biomaterial interactions of C. albicans. (a) Schematic of the biofilm model used to grow *C. albicans* biofilms over the samples under cyclic mechanical loading for 24 h. (b) Microbiological evaluations of *C. albicans* biofilms cultivated on the biomaterial surface with and without repetitive loading, including (b) biofilm biomass, (c) metabolic activity, and (d) cell viability (CFU). (e) Fluorescence microscopy z-stack images of *C. albicans* biofilms. Samples were stained with SYTO 9 (green) and propidium iodide (red) to indicate live and dead fungi, respectively. For all evaluations, the applied mechanical load (5 N) corresponds to an electrical charge of 8.5 pC/cm^2 in the piezoelectric PMMA composite.

The error bars were obtained from $N = 4$ samples. Significant differences between groups are expressed as follows: $*p < 0.05$, $**p < 0.001$, or $***p < 0.0001$.

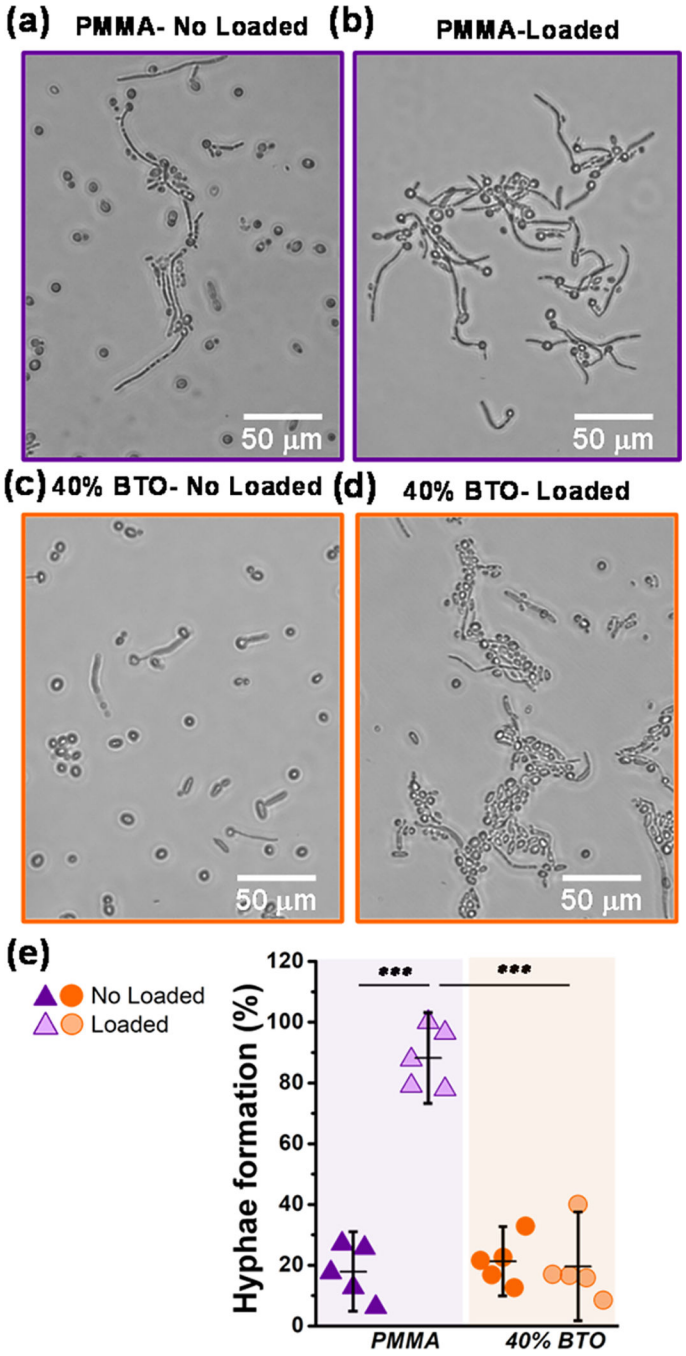

Figure 3.

Yeast-to-hyphae transition. Photomicrographs showing the morphology of *C. albicans* when in contact with (a) PMMA-no-load (control group), (b) PMMA under cyclic loading, (c) piezoelectric composite no-load, and (d) piezoelectric composite with a repetitive load. In picture (b), we can observe a predominance of hyphae morphology compared to the other groups in which yeast cells predominated (a–c), demonstrating that piezoelectric charges interfered with the morphological transition of *C. albicans*, inhibiting hyphal formation. (e) Percentage of hyphae formation after 4 h of incubation. The error bars were obtained from *N*

= 6 measurements. Significant differences between the groups are expressed as follows: *$p <$ 0.05, **$p < 0.001$, or ***$p < 0.0001$.

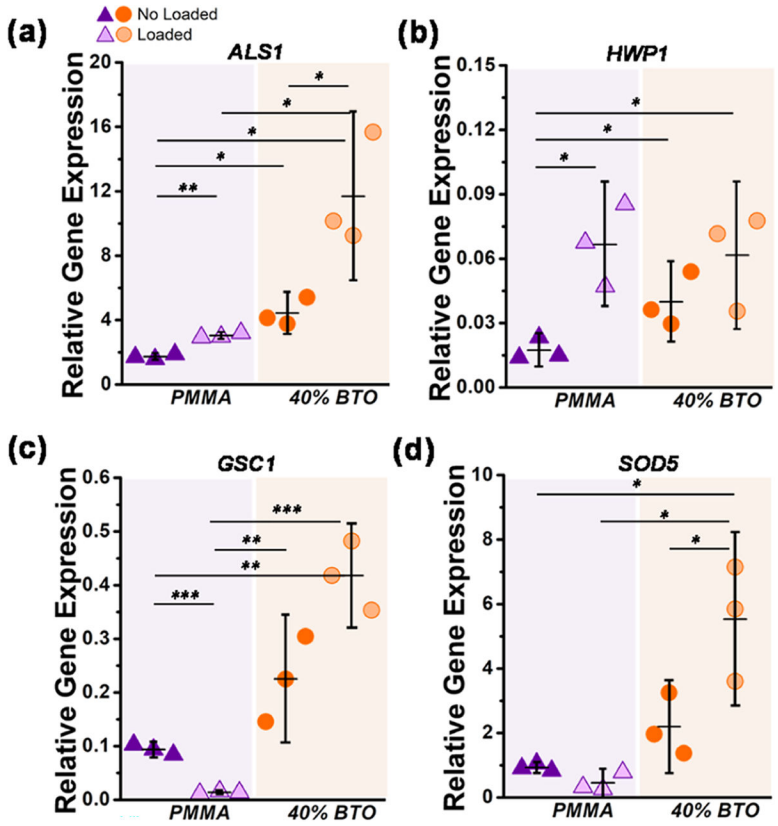

Figure 4.

Changes in the expression of genes related to the biofilm formation of C. albicans. (a) *ALS1* encoding cell-surface associated glycoproteins, (b) *HWP1* related to hyphal-specific adhesion, (c) *GSC1* involved in the β-1,3-glucan synthesis and extracellular matrix production, and (d) *SOD5* associated with superoxide dismutase production and oxidative responses. The relative gene expression was normalized to 18S ribosomal RNA levels (housekeeping). The error bars were obtained from $N = 3$ measurements. Significant differences between the groups are expressed as follows: $*p < 0.05$, $**p < 0.001$, or $***p < 0.0001$.